2017

Imaging early embryonic calcium activity with GCaMP6s transgenic zebrafish

Jiakun Chen
Washington University School of Medicine in St. Louis

Li Xia
Washington University School of Medicine in St. Louis

Michael R. Bruchas
Washington University School of Medicine in St. Louis

Lilianna Solnica-Krezel
Washington University School of Medicine in St. Louis

Developmental Biology 430 (2017) 385–396

Contents lists available at ScienceDirect

Developmental Biology

journal homepage: www.elsevier.com/locate/developmentalbiology

Imaging early embryonic calcium activity with GCaMP6s transgenic zebrafish

Jiakun Chen[a], Li Xia[b,c], Michael R. Bruchas[b,c,d], Lilianna Solnica-Krezel[a,*]

[a] Department of Developmental Biology, Washington University School of Medicine, St. Louis, MO 63110, USA
[b] Department of Anesthesiology, Division of Basic Research, Washington University School of Medicine, St. Louis, MO 63110, USA
[c] Department of Biomedical Engineering, Washington University in St. Louis, St Louis, MO, 63105, USA
[d] Department of Neuroscience, Washington University in St. Louis, St. Louis, MO, USA

ARTICLE INFO

Keywords:
Calcium transients
Embryonic cleavages
Gastrulation
Dorsal forerunner cells
β-catenin
Nodal

ABSTRACT

Intracellular Ca^{2+} signaling regulates cellular activities during embryogenesis and in adult organisms. We generated stable *Tg[βactin2:GCaMP6s]*^{stl351} and *Tg[ubi:GCaMP6s]*^{stl352} transgenic lines that combine the ubiquitously-expressed Ca^{2+} indicator GCaMP6s with the transparent characteristics of zebrafish embryos to achieve superior *in vivo* Ca^{2+} imaging. Using the *Tg[βactin2:GCaMP6s]*^{stl351} line featuring strong GCaMP6s expression from cleavage through gastrula stages, we detected higher frequency of Ca^{2+} transients in the superficial blastomeres during the blastula stages preceding the midblastula transition. Additionally, GCaMP6s also revealed that dorsal-biased Ca^{2+} signaling that follows the midblastula transition persisted longer during gastrulation, compared with earlier studies. We observed that dorsal-biased Ca^{2+} signaling is diminished in ventralized *ichabod/β-catenin2* mutant embryos and ectopically induced in embryos dorsalized by excess β-catenin. During gastrulation, we directly visualized Ca^{2+} signaling in the dorsal forerunner cells, which form in a Nodal signaling dependent manner and later give rise to the laterality organ. We found that excess Nodal increases the number and the duration of Ca^{2+} transients specifically in the dorsal forerunner cells. The GCaMP6s transgenic lines described here enable unprecedented visualization of dynamic Ca^{2+} events from embryogenesis through adulthood, augmenting the zebrafish toolbox.

1. Introduction

Ca^{2+} ion plays an important role as a second messenger to regulate cellular activity during embryogenesis and in adult organisms. An increase in intracellular Ca^{2+} concentration is generated via a receptor-mediated Ca^{2+} influx from the external space or through Ca^{2+} release from internal stores (Berridge, 1993; Clapham, 1995; Streb et al., 1983). Once intracellular Ca^{2+} concentration is elevated, Ca^{2+}-sensitive proteins, including calmodulin-dependent kinase, protein kinase C, and nuclear factor of activated T cells, can be activated to trigger different cellular responses, such as gene transcription, cell motility, and proliferation (Berridge et al., 2003; Clapham, 2007; De Koninck and Schulman, 1998; Dolmetsch et al., 1998; Gallo et al., 2006; Li et al., 1998; Oancea and Meyer, 1998).

Ca^{2+} signaling is involved in the control of many aspects of early development, including egg activation, cell cleavage, axial patterning, and morphogenesis (Webb and Miller, 2003; Whitaker, 2006). Ca^{2+} waves that propagate over the cell or the embryo were first described during fertilization in Medaka fish and sea urchin (Gilkey et al., 1978; Steinhardt et al., 1977). Subsequent studies suggested Ca^{2+} waves during fertilization are conserved in other organisms (Dumollard and Sardet, 2001; Lee et al., 1999; Runft et al., 2002; Uchida et al., 2000). Following fertilization, several aspects of embryonic cleavages are also regulated by Ca^{2+} signaling, including mitotic chromosome separation, nuclear envelope breakdown, and cytokinesis (Chang and Meng, 1995; Groigno and Whitaker, 1998; Miller et al., 1993; Parry et al., 2005). At later developmental stages, there is evidence that Ca^{2+} signaling is essential in axial patterning and cell migration (Blaser et al., 2006; Kume et al., 1997; Slusarski et al., 1997a; Wallingford et al., 2001; Westfall et al., 2003a). Recent studies also implicate Ca^{2+} signaling in the specification of left-right asymmetry during vertebrate embryogenesis (Garic-Stankovic et al., 2008; McGrath et al., 2003; Sarmah et al., 2005; Schneider et al., 2008; Takao et al., 2013; Yuan et al., 2015).

The translucent nature and rapid external development of the zebrafish embryo make it a particularly attractive model to study Ca^{2+} signaling during vertebrate embryogenesis. One-celled zebrafish zygote undergoes several synchronous cleavages to form a mound of blastomeres atop a large yolk cell (Kimmel et al., 1995). Ca^{2+} signaling

* Corresponding author.
E-mail address: solnical@wustl.edu (L. Solnica-Krezel).

http://dx.doi.org/10.1016/j.ydbio.2017.03.010
Received 9 September 2016; Received in revised form 12 January 2017; Accepted 11 March 2017
Available online 18 March 2017

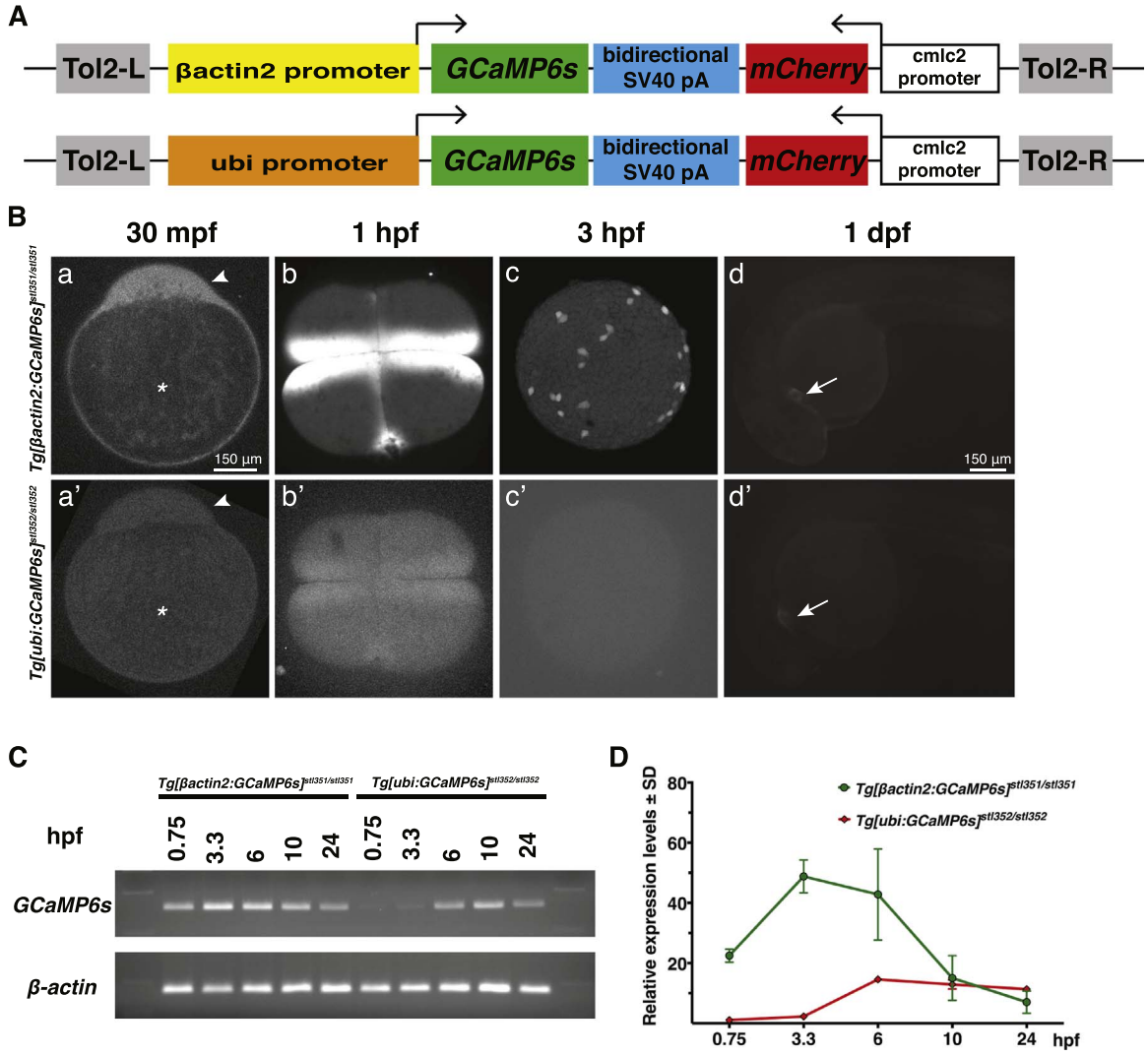

Fig. 1. GCaMP6s expression and fluorescence in *Tg[βactin2:GCaMP6s]*$^{stl351/stl351}$ and *Tg[ubi:GCaMP6s]*$^{stl352/stl352}$ transgenic zebrafish during early embryogenesis. (A) Schematics of the *Tol2[βactin2:GCaMP6s]* or *Tol2[ubi:GCaMP6s]* constructs. (B) GCaMP6s fluorescent confocal microscope images in *Tg[βactin2:GCaMP6s]*$^{stl351/stl351}$ and *Tg[ubi:GCaMP6s]*$^{stl352/stl352}$ embryos at several developmental stages. a, a', d, d', lateral view; b, b', c, c', animal pole view. Asterisks indicate the yolk, and arrowheads point to the blastodisc in a, a'. Arrows point to the heart in d, d'. (C-D) RT-PCR and qRT-PCR analyses of *GCaMP6s* RNA expression levels in *Tg[βactin2:GCaMP6s]*$^{stl351/stl351}$ and *Tg[ubi:GCaMP6s]*$^{stl352/stl352}$ embryos in the course of embryogenesis. The qRT-PCR results were normalized to *β-actin*. Error bars represent standard deviation; N=3.

is essential for cytokinesis at these cleavage stages, as injection of Ca^{2+} chelator, BAPTA, inhibits cytokinesis (Chang and Meng, 1995). Subsequent reports demonstrated that localized Ca^{2+} transients accompany initiation, propagation, and deepening of the cytokinetic furrow during the early cleavages (Webb et al., 1997). At about 64- to 128-cell stage, a different pattern of Ca^{2+} signaling emerges in the superficial blastomeres that form the enveloping layer (EVL). Transient increases of Ca^{2+} activity in the cytoplasm of EVL cells, or Ca^{2+} transients, occur uniformly across the EVL until midblastula transition (MBT) at 3 h post fertilization (hpf), when they display a transient dorsal bias, becoming barely detectable an hour later (Ma et al., 2009; Reinhard et al., 1995). Several studies have shown that disruption of Ca^{2+} release during the early blastula stage preceding MBT leads to dorsalized phenotypes, and revealed an essential role of Ca^{2+} signaling in negatively regulating β-catenin, a key mediator of embryonic axis specification (Westfall et al., 2003b; Wu et al., 2012). Similar perturbations of Ca^{2+} release performed during gastrulation implicated Ca^{2+} signaling in normal behavior of dorsal forerunner cells (DFCs), the precursors of the left-right asymmetry organ, and consequently for left-right laterality establishment (Schneider et al., 2008). Additionally, depletion of Ca^{2+} signaling during *Xenopus* gastrulation inhibits convergence and extension movements (Wallingford et al., 2001).

Despite the established importance of Ca^{2+} signaling in embryogenesis, our understanding of its spatiotemporal dynamics is limited as most of the previous studies employed either synthetic Ca^{2+} dyes or bioluminescent protein Aequorin for transient monitoring of Ca^{2+} signaling (Chang and Meng, 1995; Fluck et al., 1991; Reinhard et al., 1995; Slusarski et al., 1997b; Webb et al., 1997). Genetically encoded Ca^{2+} indicators (GECI) afford more stable and cell-type specific tools for long-term monitoring of Ca^{2+} activity (Miyawaki et al., 1997; Romoser et al., 1997). In particular, transgenic animals expressing GECI possess superior potential for imaging Ca^{2+} activity at later developmental stages or in specific cell types (Dreosti et al., 2009; Tallini et al., 2006). However, such GECIs usually suffer from lower sensitivity and slower turnover than commonly used synthetic Ca^{2+} dyes. The recently engineered GECI, GCaMP6s, shows higher sensitivity compared to commonly used synthetic Ca^{2+} dyes in mammalian and zebrafish neurons (Chen et al., 2013), providing an unprecedented tool with which to study Ca^{2+} dynamics *in vivo*. For example, GCaMP6s expressed selectively in Mauthner neurons in transgenic zebrafish enabled analysis of subcellular Ca^{2+} dynamics during startle behavior, revealing that decreased dendritic excitability underlies startle habituation (Marsden and Granato, 2015).

Here we combine the ultra-sensitivity of GCaMP6s together with

the established ubiquitous activity of *β-actin2 (βactin2)* and *ubiquitin B (ubi)* gene promoters (Kwan et al., 2007; Mosimann et al., 2011), to generate stable transgenic lines that exhibit ubiquitous GCaMP6s expression for improved *in vivo* Ca^{2+} imaging throughout early embryogenesis. Leveraging the *GCaMP6s* stable transgenic lines and the remarkable transparency of zebrafish embryos, we detected higher

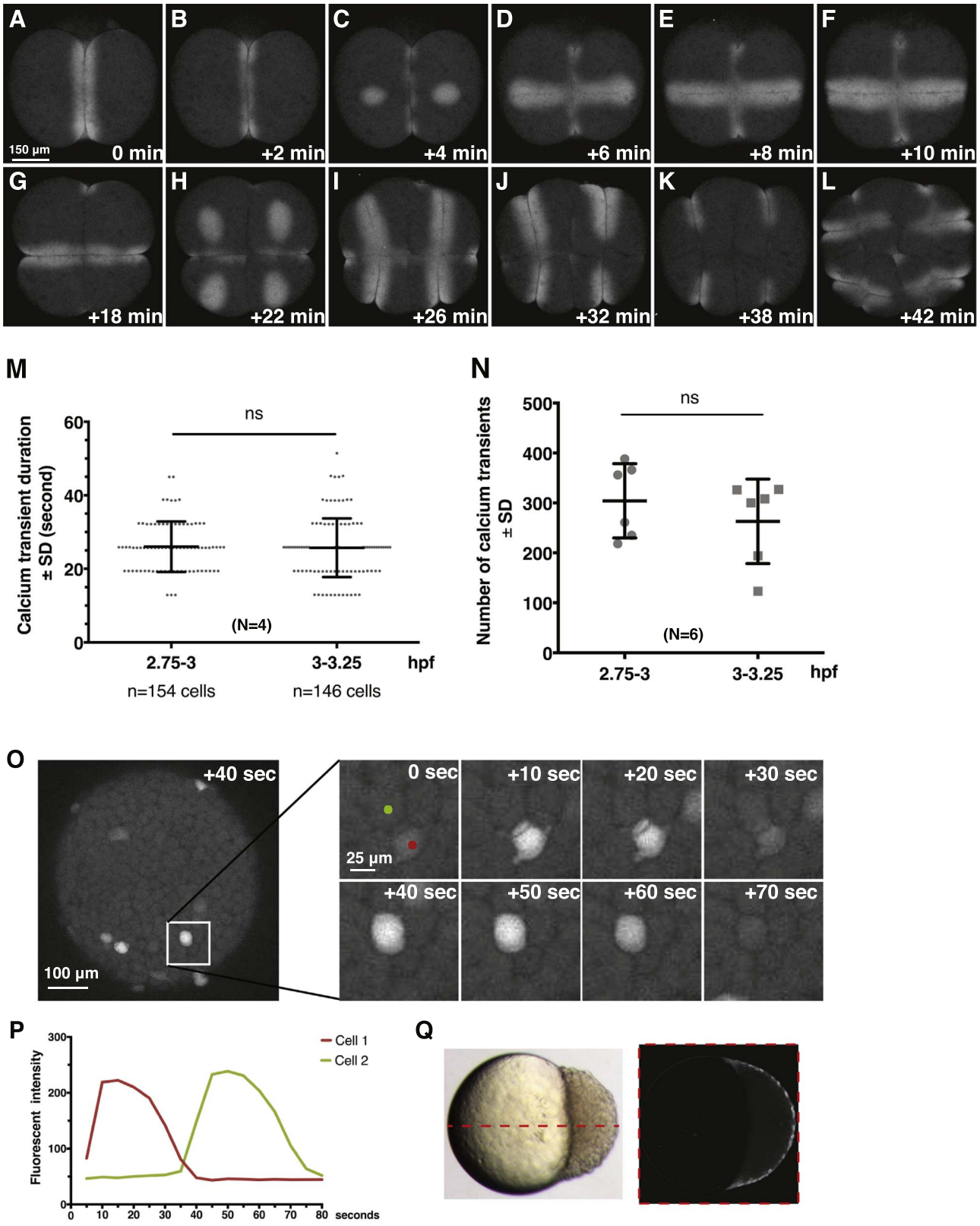

Fig. 2. Dynamics of Ca^{2+} signaling in *Tg[βactin2:GCaMP6s]*$^{stl351/stl351}$ embryos at cleavage and blastula stages. (A-L) Still images of GCaMP6s signals during cleavage furrow progression from 2-cell stage to 16-cell stage. (M) Quantification of Ca^{2+} transient duration before and after MBT. Error bars represent standard deviation; N=4 embryos. ns, not significant. (N) Comparison of Ca^{2+} transient numbers before and after MBT; N=6 embryos. (O-P) Still images and traces of Ca^{2+} transients in a time-lapse series at blastula stages. (Q) Time-lapse overlay of GCaMP6s signal from 3.7 hpf to 4 hpf from a single z-section in lateral view.

frequency of Ca^{2+} transients in the EVL cells during the early blastula stage than previously reported (Ma et al., 2009; Reinhard et al., 1995). Whereas we corroborate previous observations that the EVL Ca^{2+} transients occur more frequently on the dorsal side of the blastoderm soon after MBT (Ma et al., 2009), we show they still persist during gastrulation. Strengthening a causative link between the dorsally-biased calcium signaling window following MBT and axis formation, we also demonstrate that the dorsal-biased Ca^{2+} signaling is not

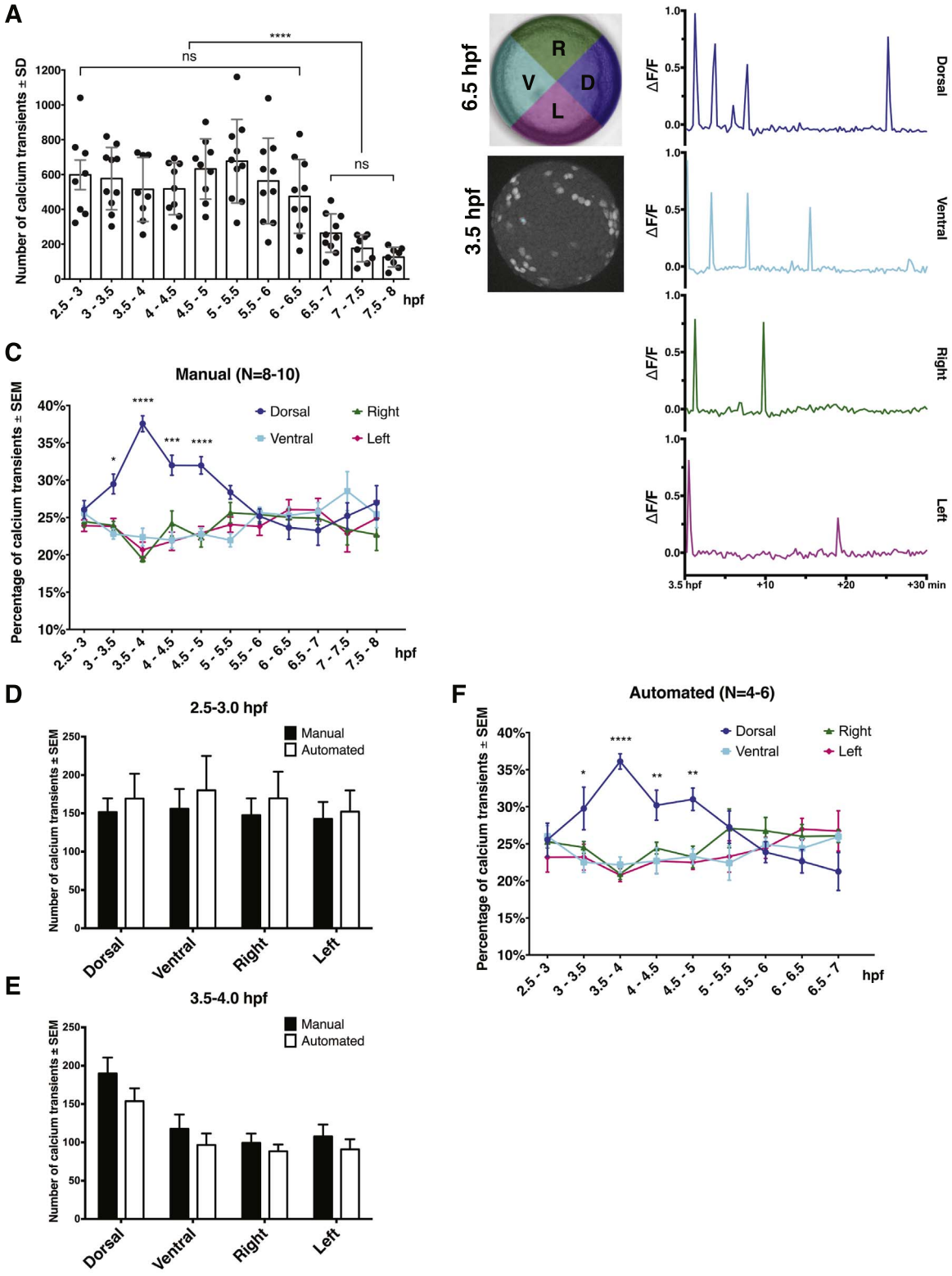

Fig. 3. Dorsal bias of the EVL Ca^{2+} transients from midblastula to late blastula stage. (A) Quantification of total Ca^{2+} transient numbers at 30-min intervals from 2.5 hpf to 8 hpf. Error bars represent standard deviation; ns, not significant. ****; P≤0.0001; N=8–10 embryos. (B) Representative Ca^{2+} transient traces from a single spot in each quadrant between 3.5 hpf and 4 hpf. (C) Manual quantification of Ca^{2+} transient frequency in four blastoderm quadrants from 2.5 hpf to 8 hpf; N=8–10 embryos. (D). Comparisons of Ca^{2+} transient numbers in individual quadrant between manual and automated quantifications at 2.5–3 hpf and 3.5–4 hpf. (E) Automated quantification of Ca^{2+} transient frequency from 2.5 hpf to 7 hpf. Error bars represent S.E.M. *, P≤0.05. ***, P≤0.001. ****, P≤0.0001; N=4–6 embryos.

observed in ventralized *ichabod/β-catenin2* mutant embryos and is ectopically induced in embryos dorsalized by excess β-catenin. We further report direct visualization of Ca^{2+} signaling in individual DFCs during gastrulation and show that their duration can be modulated by Nodal signaling. The GCaMP6s transgenic lines described here will enable visualization of additional dynamic Ca^{2+} events at embryonic and larval stages as well as in adult animals and thus augment the zebrafish toolbox.

2. Results

2.1. Generation and characterization of Tg[βactin2:GCaMP6s]^{stl351} and Tg[ubi:GCaMP6s]^{stl352} transgenic zebrafish

To enable highly sensitive and dynamic monitoring of Ca^{2+} signaling throughout zebrafish development, we generated GCaMP6s transgenic lines using the Tol2 transposon method as previously described (Kawakami et al., 2000; Maximiliano et al., 2009). Towards imaging maternal and early embryonic Ca^{2+} activity, we employed *βactin2* and *ubi* promoters to drive GCaMP6s expression ubiquitously (Fig. 1A). To establish stable transgenic lines with a single insertion, we screened for F1 carriers that produced 50% GCaMP6s-positive F2 progeny and recovered candidate lines with single *GCaMP6s* integration for both promoters, referred to as *Tg[βactin2:GCaMP6s]*^{stl351} and *Tg[ubi:GCaMP6s]*^{stl352}. Both transgenic lines developed normally as heterozygotes and homozygotes and showed fecundity comparable to wild-type (WT) fish. Embryos obtained from carriers of either transgene displayed GCaMP6s fluorescence in the heart at 1 day post fertilization (dpf) (Fig. 1B), likely owing to Ca^{2+} signaling associated with cardiac conduction (Chi et al., 2010). Consistent with both transgenic lines containing a single insertion in their genomes, quantitative PCR using their genomic DNA as a template and *GCaMP6s*-specific primers revealed two-fold higher amount of *GCaMP6s* sequences in homozygous compared to hemizygous fish (Supp. Fig. 1A). Together, these results support the notion that *Tg[βactin2:GCaMP6s]*^{stl351} and *Tg[ubi:GCaMP6s]*^{stl352} represent single-integration stable transgenic lines.

Ca^{2+} signaling in the cleavage and early blastula stages of zebrafish development is observed soon after egg activation, and occurs without zygotic transcription, which is initiated around MBT (Aanes et al., 2011; Harvey et al., 2013; Kane and Kimmel, 1993; Lee et al., 2013). Hence, we reasoned detecting Ca^{2+} activity at these early stages would require sufficiently high levels of maternally-deposited GCaMP6s protein and/or mRNA in the eggs. Although both *βactin2* and *ubi* promoters have been reported to drive ubiquitous expression during zebrafish embryogenesis, their activities at the early developmental stages have not been yet carefully characterized (Kwan et al., 2007; Mosimann and Zon, 2011). To compare the activities of these two transgenic lines, we first imaged transgenic embryos at various stages using confocal microscopy. At 30 min post fertilization (mpf), Ca^{2+} activity was clearly detected in the cytoplasmic blastodisc of *Tg[βactin2:GCaMP6s]*$^{stl351/stl351}$ zygotes (Fig. 1Ba). By contrast, only weak Ca^{2+} signaling could be detected in *Tg[ubi:GCaMP6s]*$^{stl352/stl352}$ zygotes under the same imaging conditions (Fig. 1Ba'). Similarly, we detected robust Ca^{2+} signaling at cleavage and blastula stages in *Tg[βactin2:GCaMP6s]*$^{stl351/stl351}$ (Fig. 1Bb,c) but not in *Tg[ubi:GCaMP6s]*$^{stl352/stl352}$ embryos (Fig. 1Bb',c'). By contrast, we observed comparable levels of Ca^{2+} signaling in the embryonic hearts at 24 hpf (Fig. 1Bd,d') and later in the contracting muscles of moving larvae (data not shown) from either transgenic line. We hypothesized that the differences in the early GCaMP6s signal between the two transgenic lines were due to different driving activities of *βactin2* and *ubi* promoters during oogenesis. To test this, we examined the relative *GCaMP6s* mRNA levels in *Tg[βactin2:GCaMP6s]*$^{stl351/stl351}$ and *Tg[ubi:GCaMP6s]*$^{stl352/stl352}$ embryos by qRT-PCR. The results indicated that *GCaMP6s* RNA expression levels were significantly higher in *Tg[βactin2:-GCaMP6s]*$^{stl351/stl351}$ embryos than *Tg[ubi:GCaMP6s]*$^{stl352/stl352}$ embryos at all developmental stages before 10 hpf, whereas embryos from both transgenic lines displayed comparable *GCaMP6s* mRNA levels at later stages (Fig. 1C,D), consistent with the above results. Taken together, these data indicate that *Tg[βactin2:GCaMP6s]*$^{stl351/stl351}$ embryos have higher GCaMP6s expression than *Tg[ubi:GCaMP6s]*$^{stl352/stl352}$ embryos during the first 10 h of zebrafish development. Consequently, we employed the *Tg[βactin2:GCaMP6s]*$^{stl351/stl351}$ transgenic line for imaging Ca^{2+} signaling during early embryogenesis.

2.2. In vivo imaging of Ca^{2+} activities during cleavage stage in Tg[βactin2:GCaMP6s]$^{stl351/stl351}$ embryos

In the zebrafish zygote, early cleavages are meroblastic and occur synchronously at about 15-min intervals. The first few cell divisions follow a stereotypic pattern with the successive cleavages being oriented perpendicularly to the preceding ones (Kimmel et al., 1995). Using time-lapse spinning disk confocal microscopy (Materials and methods), we observed that GCaMP6s signal localized to the dynamic cleavage furrow, indicating that strong Ca^{2+} activity accompanied the cytokinetic furrow ingression (Fig. 2A). During the transition from 2- to 4-cell stage, the GCaMP6s signals that accompanied the first furrow diminished and eventually disappeared (Fig. 2B,C). Meanwhile, GCaMP6s fluorescence was detected in the equatorial cortex of the nascent cleavage furrows in the currently dividing blastomeres (Fig. 2C). Subsequently, GCaMP6s signals propagated across the future division plane laterally, and extended with the furrow progression (Fig. 2D-G). This furrow-associated Ca^{2+} signaling could be detected in *Tg[βactin2:GCaMP6s]*$^{stl351/stl351}$ embryos in the following cell cycles until 32-cell or 64-cell stages (Fig. 2H-L, Movie S1), but later became undetectable, consistent with previous reports (Webb et al., 1997). The dynamic Ca^{2+} signaling during the cleavage stages is consistent with Ca^{2+} playing a critical role in embryonic cleavages.

Supplementary material related to this article can be found online at doi:10.1016/j.ydbio.2017.03.010.

2.3. In vivo imaging of Ca^{2+} activities in Tg[βactin2:GCaMP6s]$^{stl351/stl351}$ blastulae

Time-lapse analyses of *Tg[βactin2:GCaMP6s]*$^{stl351/stl351}$ transgenic embryos during the blastula stage (2–3 hpf) revealed cytoplasmic Ca^{2+} transients (Fig. 1Bc), which occur uniformly across the blastoderm in individual and nondividing blastomeres (Fig. 3C,D). The Ca^{2+} transients initiated at around 64- to 128-cell stages and had an average duration of about 20–30 s (25.83 ± 7.50 s, N=4 embryos; Fig. 2M), consistent with previous studies (Ma et al., 2009; Reinhard et al., 1995). However, our analyses revealed more frequent Ca^{2+} transients than previously reported (304.0 ± 84.6 at 2.75–3 hpf, N=6 embryos) (Fig. 2N). We also noticed Ca^{2+} transients in a single cell sometimes were associated with Ca^{2+} signals appearing in nearby cells. Such coordinated Ca^{2+} transients usually were restricted to neighboring cells that were one- or two- cells apart, consistent with the suggested transmission of Ca^{2+} signaling between blastomeres at this stage of development (Ma et al., 2009) (Fig. 2O,P, Movie S2). Since GCaMP6s displays superior Ca^{2+} sensitivity (Chen et al., 2013 and this work), we tested whether Ca^{2+} transients could be detected also in the deep cells of the *Tg[βactin2:GCaMP6s]*$^{stl351/stl351}$ embryos. Against this notion, our time-lapse analyses failed to reveal any Ca^{2+} transients in the deep cells (Fig. 2Q).

Supplementary material related to this article can be found online at doi:10.1016/j.ydbio.2017.03.010.

We next wanted to test the sensitivity of *Tg[βactin2:GCaMP6s]*$^{stl351/stl351}$ transgenic line upon ectopic Ca^{2+} activation. Therefore, we injected synthetic RNA encoding mCherry and Wnt5b, the latter has been implicated in the regulation

of EVL Ca^{2+} transients during blastula stage (Lin et al., 2010; Slusarski et al., 1997a, 1997b). Interestingly, we observed an increased number of Ca^{2+} transients in Wnt5b-misexpressing embryos before MBT but not after, as the number of Ca^{2+} transients became comparable to that in control embryos injected with *mCherry* RNA after 3 hpf (Supp. Fig. 2A, N=5 embryos each). However, the fluorescence intensity was constantly higher in *wnt5b* RNA-injected embryos compared to control embryos across the time period examined (2.5–4 hpf) albeit it slightly decreased at 3.5–4 hpf (Supp. Fig. 2B,C). In addition, after MBT, *wnt5b* RNA-injected embryos displayed a similar pattern of dorsal-biased Ca^{2+} signaling to that observed in control embryos (Supp. Fig. 2D) and uninjected embryos (Fig. 3C,F).

Together, our studies of *Tg[βactin2:GCaMP6s]*$^{stl351/stl351}$ revealed that Ca^{2+} transients occur at higher frequency in the early zebrafish blastula than previously shown, but provided further support for the notion that Ca^{2+} transients are restricted to the EVL cells and occur uniformly across the blastoderm at this stage of development (Ma et al., 2009; Reinhard et al., 1995). Moreover, Ca^{2+} transients' frequency before MBT can be increased by excess Wnt5b (Lin et al., 2010).

2.4. Comparison of EVL Ca^{2+} transients during blastula and gastrula stage

Given the relatively low sensitivity and transient expression of the Ca^{2+} sensors employed in previous studies (Reinhard et al., 1995; Webb and Miller, 2003), we wondered whether we could detect Ca^{2+} transients at later stages with the *Tg[βactin2:GCaMP6s]*$^{stl351/stl351}$ transgenic

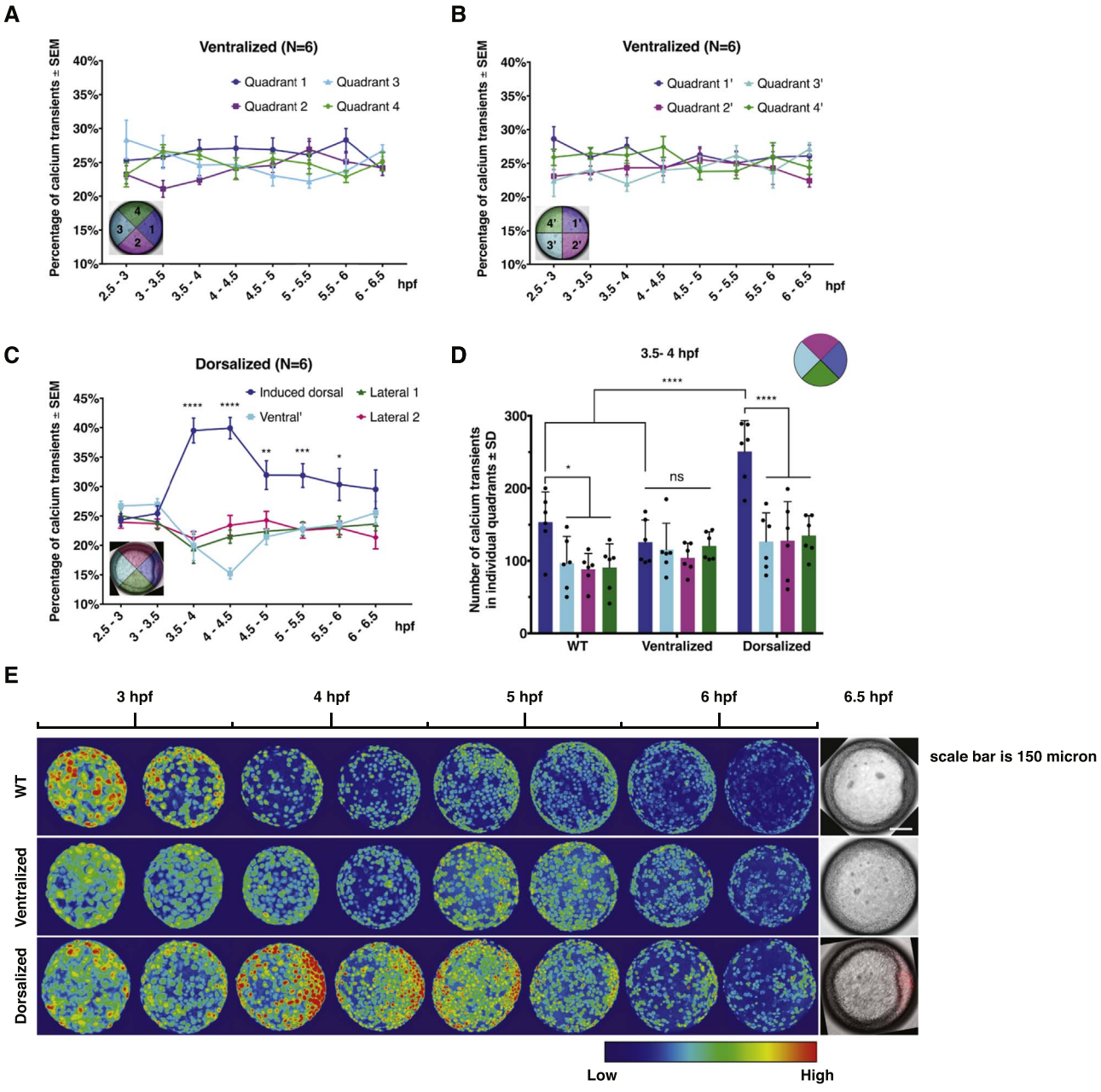

Fig. 4. EVL Ca^{2+} signaling pattern in ventralized and dorsalized embryos. (A-B) Automated quantification of EVL Ca^{2+} transient frequency in *ichabod/β-catenin2* ventralized embryos between 2.5 hpf and 6.5 hpf. Error bars represent S.E.M.; N=6 embryos. (C) Automated quantification of EVL Ca^{2+} transient frequency in *β-catenin1*-injected dorsalized embryos. Induced dorsal organizer is oriented to the right. Error bars represent S.E.M. *, P≤0.05. **, P≤0.01***, P≤0.001. ****, P≤0.0001; N=6 embryos. (D) Comparison of Ca^{2+} transient number in individual quadrants among WT, ventralized, and dorsalized embryos at 3.5–4 hpf. Error bars represent standard deviation. ns, not significant. *, P≤0.05. ****, P≤0.0001; (E) Representative 30-min time-lapse overlay of GCaMP6s signals in WT, ventralized, and dorsalized embryos from 2.5 hpf to 6.5 hpf.

line. To this end, we carried out long-term time-lapse confocal microscopy analyses of Ca^{2+} activity from the MBT through mid-gastrulation stages (2.5–8.0 hpf). We observed comparable Ca^{2+} transients albeit of decreasing frequency throughout blastula and early gastrula stages (598.1 ± 240.1 at 2.5–3 hpf compared to 474.3 ± 212.4 at 6–6.5 hpf). Like during blastula stages, our imaging approach only detected Ca^{2+} transients in the EVL cells of the *Tg[βactin2:GCaMP6s]*$^{stl351/stl351}$ gastrulae. From 6.5 hpf the number of Ca^{2+} transients in the EVL further decreased over time (263.1 ± 110.1 at 6.5–7 hpf) but still persisted to the end of the imaging period at 8 hpf (Fig. 3A, Movie S3). Interestingly, this reduction of Ca^{2+} transient frequency occurs soon after the dorsal organizer, or embryonic shield is established at 6 hpf (Kimmel et al., 1995).

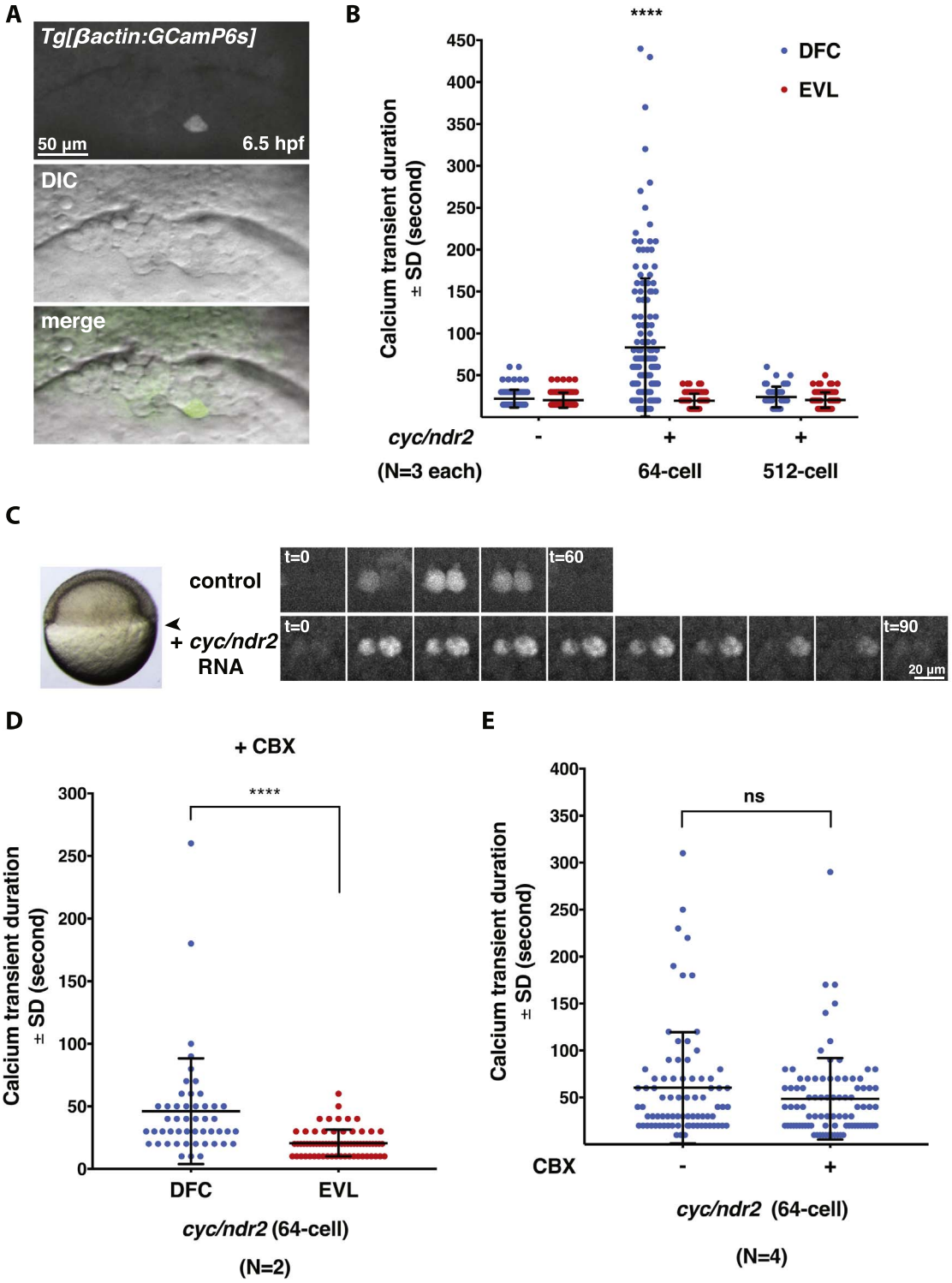

Fig. 5. Excess Nodal signaling prolongs Ca^{2+} transient duration specifically in the DFCs. (A) Representative images of a single Ca^{2+} transient in a DFC at 6.5 hpf. (B) Quantification of Ca^{2+} transient duration in WT and Cyc/Ndr2-misexpressing embryos. Error bars represent standard deviation. ****, P≤0.0001. N=3 embryos in control and Cyc/Ndr2-misexpressing embryos, respectively. (C) Still images of Ca^{2+} transients in the DFCs of uninjected control and Cyc/Ndr2-misexpressing embryo in a time-lapse series. Arrowhead points to the DFC region that was imaged. (D) Quantification of DFC Ca^{2+} transient duration between DFCs and EVL cells in *cyc/ndr2* RNA-injected embryos after CBX treatment. ****, P≤0.0001. N=2 embryos. (E) Quantification of DFC Ca^{2+} transient duration in Cyc/Ndr2-misexpressing embryos before and after CBX treatment. ns, not significant; N=4 embryos.

Supplementary material related to this article can be found online at doi:10.1016/j.ydbio.2017.03.010.

Whereas the EVL Ca^{2+} transients occur homogeneously across the entire EVL before the MBT, they later display a dorsal-biased Ca^{2+} signaling window after MBT (3–4 hpf) (Ma et al., 2009). To corroborate such observations, we manually quantified Ca^{2+} transients in each individual quadrant (dorsal, ventral, right, and left, identified retrospectively) in a 30-min time interval from 2.5 hpf to 8 hpf (Fig. 3B, and also see Materials and methods). These analyses showed that a higher frequency of Ca^{2+} transients in the dorsal compared to the other three quadrants initiated at 3 hpf and lasted until 5 hpf. Subsequently, Ca^{2+} transients occurred at a similar frequency in all quadrants throughout the remaining stages analyzed (Fig. 3C, N=8–10 embryos).

To avoid any bias of manual analysis, we also developed an automated algorithm for the Ca^{2+} transient quantification (Materials and methods). To ensure the reliability of this method, we first compared the total number of Ca^{2+} transients between manual and automated quantification before and after the establishment of the dorsal-biased Ca^{2+} signaling. The results indicated that the two methods detected a comparable number of Ca^{2+} transients at both stages, and revealed a similar relative increase of Ca^{2+} transients in the dorsal quadrant at 3.5–4 hpf (Fig. 3D,E). We further carried on the analyses from 2.5 hpf to 7 hpf using the automated method, which revealed dorsally enriched Ca^{2+} activity between 3 and 5 hpf, consistent with our manual quantification (Fig. 3C,F, N=4–6 embryos).

Together, we found that the EVL Ca^{2+} transients persist during blastula and gastrula stages, and display a two-hour dorsal-biased enrichment (3–5 hpf) preceding the morphological manifestation of the dorsal organizer, or formation of the embryonic shield, that occurs at 6 hpf (Kimmel et al., 1995). Further, the total frequency of EVL Ca^{2+} transients starts to decrease following the embryonic shield establishment.

2.5. Characterization of EVL Ca^{2+} activities in ventralized and dorsalized embryos

The dorsal-biased Ca^{2+} signaling observed following MBT (Ma et al., 2009; this work), suggests a correlation between EVL Ca^{2+} signaling and the establishment of dorsal organizer or embryonic shield, which is manifested morphologically at 6 hpf. One prediction of such a correlation is that the Ca^{2+} dynamics should be altered in embryos with defective dorsoventral patterning. To test this, we first imaged EVL Ca^{2+} transients from 2.5 hpf to 6.5 hpf in maternal zygotic *ichabod/β-catenin2* ventralized embryos (Kelly et al., 2000). As we could not define morphologically the dorsal region in ventralized embryos, which lack the embryonic shield (Kelly et al., 2000), we randomly divided mutant embryos into quadrants in two different ways (Fig. 4A,B). Our analyses showed no significant bias toward any quadrant across the time window analyzed (Fig. 4A, B, N=6 embryos).

To test EVL Ca^{2+} signaling in dorsalized embryos, we injected *β-catenin1/H2b-RFP* synthetic RNA to one of the marginal cells at 8–16 cell stage (Kelly et al., 1995). Expression of H2b-RFP allowed identification of the induced dorsal organizer by examining H2b-RFP expression (Fig. 4C). Using the H2b-RFP expression and embryonic shield morphology, we defined the induced dorsal quadrant and the other three quadrants disregarding any endogenous dorsal organizer or embryonic shield. The automatic analysis of Ca^{2+}transients showed that the frequency of Ca^{2+} transients was significantly higher in the induced dorsal quadrant than the other three quadrants in a fashion similar to that observed in WT embryos (Fig. 4C, N=6 embryos versus Fig. 3C,F). It is noteworthy that the total number of Ca^{2+} transients was comparable in ventralized and dorsalized embryos to that detected in WT embryos (Fig. 4E, Supp. Fig. 3A). Whereas the induced dorsal quadrant showed a higher number of Ca^{2+} transients than WT dorsal quadrant at 3.5–4 hpf (Fig. 4D, Supp. Fig. 3B), we have not detected significant difference in the number of transients in non-dorsal quadrants in dorsalized versus WT embryos at 3.5–4 hpf. Collectively, these data indicate that the biased-EVL Ca^{2+} signaling that is initiated soon after MBT is strongly associated with and an early predictor of the dorsal organizer formation.

2.6. Characterization of dorsal forerunner cell Ca^{2+} activity in Tg[βactin2:GCaMP6s]$^{stl351/stl351}$

Dorsal forerunner cells (DFCs) form by ingression of dorsal marginal EVL cells at the onset of epiboly (Oteiza et al., 2008). In the course of epiboly, they move vegetally ahead of the deep cell margin while remaining closely associated with the overlying EVL margin, earning their name DFCs (Solnica-Krezel et al., 1996). At early somitogenesis, the DFCs organize to form a ciliated epithelium of the Kupffer's vesicle (KV), a transient structure essential for left-right patterning (Amack and Yost, 2004; Essner et al., 2005). Ca^{2+} signaling in the DFCs during gastrulation, visualized in lateral view using dextran-conjugated Ca^{2+} sensor Fura-2, has been implicated in the control of left-right pattering (Schneider et al., 2008). However, carrying out similar time-lapse imaging of *Tg[βactin2:-GCaMP6s]$^{stl351/stl351}$* gastrulae in lateral view, we found it difficult to discern whether the GCaMP6s signals originate from the DFCs or the adjacent thin EVL cells. Instead, using time-lapse confocal imaging, Ca^{2+} transients in the DFCs were clearly detected in dorsal view and could be distinguished from the EVL Ca^{2+} transients due to the smaller size and rounder shape of DFCs compared to the large, flat and polygonal EVL cells (Fig. 5A). The Ca^{2+} transients in DFCs exhibited a similar duration to those observed in EVL cells (Fig. 5B), and were visible from the shield to 90% epiboly stage (6–9 hpf) (data not shown). These data are consistent with the previous work (Schneider et al., 2008), but provide a direct evidence for Ca^{2+} activity in the DFCs.

Nodal signaling has an instructive role in DFC formation: overexpression of the Nodal ligand Cyclops/Nodal-related 2 (Cyc/Ndr2) strongly increases the DFC numbers, whereas the deficiency of Nodal signaling results in DFC deficiency (Choi et al., 2007; Oteiza et al., 2008). To test whether supranumerary DFCs induced by excess Nodal signaling exhibit normal Ca^{2+} activity, we performed time-lapse confocal imaging of *Tg[βactin2:GCaMP6s]$^{stl351/stl351}$* embryos injected at 64-cell stage with *cyc/ndr2* synthetic RNA. We observed numerous ectopic DFCs in the *cyc/ndr2* RNA-injected embryos, and a proportional expansion of Ca^{2+} transients in the injected embryos (Movie S4). Surprisingly, we also observed prolonged duration of Ca^{2+} transients in individual DFCs in the Cyc/Ndr2-overexpressing gastrulae with an average Ca^{2+} transient lasting 83.33 ± 6.7 s (n=150 cells in N=3 embryos), compared to 22.16 ± 1.1 s (n=88 cells in N=3 embryos) in DFCs from control gastrulae (Fig. 5B,C). By contrast, the EVL cells in the *cyc/ndr2* RNA-injected embryos displayed comparable duration of Ca^{2+} transients to those in control gastrulae (Fig. 5B). These data indicate that enhanced Nodal signaling is sufficient to increase Ca^{2+} transients in the DFC domain, likely due to supernumerary DFCs. In addition, excess Nodal signaling increases Ca^{2+} transient duration specifically in the DFCs without affecting the duration of Ca^{2+} transients in the EVL cells. We next wished to determine whether Nodal signaling could directly influence Ca^{2+} transient duration in DFCs. Therefore, we injected *cyc/ndr2* RNA at 512-cell stage into the yolk cell after it becomes separated from the blastoderm, but the yolk-injected RNA can be selectively targeted to the DFCs owing to their unique endocytic activity (Cooper and D'Amico, 1996). Although we observed dorsalized phenotypes in the embryos injected with *cyc/ndr2* RNA as expected (Sampath et al., 1998), we found that DFC Ca^{2+} transients exhibited duration not significantly different from that in control embryos (Fig. 5B, N=3 embryos).

To test whether Ca^{2+}-induced Ca^{2+} release plays a role in sustaining DFC Ca^{2+} transient duration in embryos injected with *cyc/ndr2* RNA at 64-cell stage, we treated the injected embryos with a gap junction

inhibitor carbenoxolone (CBX) during gastrulation (6–6.5 hpf) before time-lapse imaging (Satou et al., 2009; Wang et al., 2014; Yin et al., 2012). We found the elongated Ca^{2+} transients duration still persisted specifically in the DFCs but not in the EVL cells (Fig. 5D, N=2 embryos), despite severe epiboly defects exhibited by the treated-embryos (Movie S5). We further carried out experiments to compare Ca^{2+} transients duration before and after CBX treatment by applying CBX solution in the course of imaging. However, we still found no significant difference of DFC Ca^{2+} transient duration before or after CBX treatment in the Cyc/Ndr2-overexpressing embryos (Fig. 5E, N=4 embryos). Together, our data suggest that the DFC Ca^{2+} transient duration is influenced by Nodal signaling indirectly and is not mediated through Ca^{2+}-induced Ca^{2+} release.

Supplementary material related to this article can be found online at doi:10.1016/j.ydbio.2017.03.010.

3. Discussion

Here we report the generation of stable transgenic zebrafish lines with ubiquitous expression of GCaMP6s for improved Ca^{2+} imaging *in vivo*. Using the *Tg[βactin2: GCaMP6s]*$^{stl351/stl351}$ line, we describe enhanced Ca^{2+} imaging in the first 10 h of zebrafish embryogenesis compared to previously reported methods. We confirm and extend earlier studies of Ca^{2+} signaling activities during cleavage and early blastula stages. Whereas imaging *Tg[βactin2: GCaMP6s]*$^{stl351/stl351}$ corroborates previously described Ca^{2+} transients randomly occurring in the superficial EVL cells preceding MBT, GCaMP6s revealed that these Ca^{2+} transients occur at higher frequency than previously appreciated. The stable expression of GCaMP6s also corroborated that the EVL Ca^{2+} transients display an asymmetry toward the dorsal quadrant from midblastula to late blastula stages, when the EVL Ca^{2+} transients become uniform and persist during gastrulation. Lastly, GCaMP6s allowed direct monitoring of Ca^{2+} transients in the DFCs during gastrulation at a single cell resolution. Interestingly, we observed prolonged Ca^{2+} transients specifically in the DFCs of gastrulae overexpressing the Nodal ligand Cyc/Ndr2. Taken together, these data indicate GCaMP6s is a superior Ca^{2+} sensor for monitoring dynamic Ca^{2+} activity throughout zebrafish embryogenesis.

Our study provides a direct comparison of two zebrafish ubiquitous promoters, *βactin2* and *ubiquitin*, during early embryonic development. We present several lines of evidence that the *βactin2* promoter in *Tg[βactin2:GCaMP6s]*$^{stl351/stl351}$ transgenic line possesses stronger maternal activity to drive transgenic expression compared to the expression observed in *Tg[ubi: GCaMP6s]*$^{stl352/stl352}$ embryos. The *βactin2* promoter, which contains a 5.3-kb element upstream of the *β-actin2* gene start codon, was shown to provide broad expression throughout the embryo at 24 hpf (Kwan et al., 2007). Subsequent studies also reported ubiquitous expression of various proteins using the *βactin2* promoter (Campinho et al., 2013; Randlett et al., 2011). Zebrafish *ubi* promoter was also recently reported to drive constitutive transgene expression during developmental stages after 24 hpf (Mosimann et al., 2013; Mosimann and Zon, 2011). Here we directly compared *βactin2* and *ubi* promoters in their ability to drive GCaMP6s expression in stable transgenic lines in the first 24 h of embryogenesis. Analyzing single-copy insertion alleles for both lines, we observed that *Tg[βactin2:GCaMP6s]*$^{stl351/stl351}$ embryos exhibited more robust *GCaMP6s* RNA expression levels at stages before 10 hpf by qRT-PCR. Confocal Ca^{2+} imaging at a series of early developmental stages corroborated these results. At later developmental stages, the two transgenic lines conferred similar levels of GCaMP6s expression levels. Based on these results we propose that *βactin2* should be a promoter of choice to ensure transgene expression at blastula stages. However, the possible position effects of transgene integration on influencing GCaMP6s expression in these two transgenic lines should also be considered. Indeed, previous studies in mouse and zebrafish suggested that expression pattern of a gene inserted at the transgene integration locus may be influenced by the nearby regulatory elements (Jaenisch et al., 1981; Roberts et al., 2014; Wilson et al., 1990).

Consistent with the higher sensitivity of GCaMP6s for Ca^{2+} transient detection (Chen et al., 2013), we detected higher frequency of Ca^{2+} transients in EVL cells during the blastula stage in comparison with previous studies. In our *Tg[βactin2:GCaMP6s]*$^{stl351/stl351}$ embryos, we observed about 304.0 ± 84.6 transients per 15-min interval (2.75–3 hpf) in the blastulae. Using Aequorin-based luminescent Ca^{2+} imaging, Ma and colleagues detected about 40–80 Ca^{2+} transients per 15-min interval at the blastula stage (Ma et al., 2009), a 4–8 fold difference. Indicating that the *Tg[βactin2:GCaMP6s]*$^{stl351/stl351}$ reporter can also detect supranumerary Ca^{2+} transients, we observed increased numbers and amplitude of Ca^{2+} transients in early blastulae overexpressing Wnt5b (Supp. Fig. 2), a secreted ligand previously shown to activate calcium signaling in early zebrafish embryos (Slusarski et al., 1997b; Westfall et al., 2003a). In addition, the EVL Ca^{2+} transients in the *Tg[βactin2:GCaMP6s]*$^{stl351/stl351}$ embryos still persisted during gastrulation (Fig. 3A), contrasting previous observations in which they started to diminish at the late blastula stage (Ma et al., 2009; Reinhard et al., 1995). Given that these studies employed transient expression of either synthetic Ca^{2+} dyes (Ca^{2+} green dextran and NuCa-green) or injection of recombinant *f*-aequorin, we reasoned the stably-expressed GCaMP6s under *βactin2* promoter likely allowed us to detect the EVL Ca^{2+} transients at this relatively later developmental stage. However, we did not detect any obvious intercellular Ca^{2+} waves during the gastrula stage in *Tg[βactin2:GCaMP6s]*$^{stl351/stl351}$ embryos (Gilland et al., 1999; Webb and Miller, 2003). This discrepancy is likely due to the different imaging approach we employed in this work compared with previous studies, and further experiments are warranted to explore such large-scale Ca^{2+} activities during gastrulation. It is also possible that using in future studies other GCaMP6 variants (GCaMP6m, GCaMP6f), which provide faster kinetic sensitivity than GCaMP6s (Chen et al., 2013), might enable the detection of more transient Ca^{2+} events at this stage.

Ca^{2+} signaling has been proposed to play important roles during axis formation in vertebrates. In *Xenopus* and zebrafish, suppression of intracellular Ca^{2+} release using chemical inhibitors or interference with specific genes results in dorsalized phenotypes by negatively regulating activity of the maternal Wnt/β-catenin pathway (Kume et al., 1997; Lyman Gingerich et al., 2005; Westfall et al., 2003a). Together, these studies support the model in which the uniform Ca^{2+} transients in EVL cells during the blastula stages limit axis formation. However, it remains unclear whether Ca^{2+} signaling functions in this process in a cell autonomous or non-autonomous manner to modulate the maternal Wnt/β-catenin pathway in the zebrafish blastomeres. Whereas β-catenin has been detected in the nuclei of dorsal superficial EVL cells and deeper blastomeres (Kelly et al., 2000; Schneider et al., 1996), Reinhard and colleagues reported that Ca^{2+} signaling is nearly exclusively restricted to the EVL cells, implying that the modulation of maternal Wnt/β-catenin by Ca^{2+} transients is cell non-autonomous (Reinhard et al., 1995). Our confocal microscope analyses employing the supersensitive Ca^{2+} indicator GCaMP6s also failed to detect any Ca^{2+} activity within the deep cells in the GCaMP6s transgenic lines during the blastula stage. Thus these data corroborate the previous observation that Ca^{2+} transients indeed occur only in the EVL blastomeres (Reinhard et al., 1995), and provide further support for the cell non-autonomous mechanism of β-catenin regulation by a Ca^{2+}-dependent activity. One such molecule that could function upstream of EVL Ca^{2+} signaling is Wnt5, which has been reported to stimulate Ca^{2+} release to antagonize Wnt/β-catenin activity (Slusarski et al., 1997b; Westfall et al., 2003a). Interestingly, despite detecting increased uniform Ca^{2+} transients before MBT, we did not observe ventralized phenotypes in Wnt5b-overexpressing embryos (Supp. Fig. 2A-C and data not shown). Accordingly, we also detected in Wnt5b-overexpressing embryos the dorsal-biased Ca^{2+} signaling pattern (Supp. Fig. 2D), which is usually absent in ventralized embryos (Fig. 4A,B). Similarly,

we did not observe increased Ca^{2+} signaling before MBT in *ichabod/β-catenin2* ventralized embryos, which might be explained by the mutation directly influencing expression levels of β-catenin2 (Kelly et al., 2000), instead of an upstream regulator.

It was suggested that the establishment of dorsal-biased Ca^{2+} signaling results from reduction of Ca^{2+} transients in the other three quadrants (ventral, left, and right quadrants) following MBT (Ma et al., 2009). However, we found no significant difference in the total number of Ca^{2+} transients in the *Tg[βactin2:GCaMP6s]*$^{stl351/stl351}$ embryos before and after MBT (Fig. 2N). Instead, our results indicated the dorsal-biased Ca^{2+} signaling is due to a higher frequency of Ca^{2+} transients in the dorsal quadrant compared with other quadrants. Moreover, the number of calcium transients increased further in embryos dorsalized by injection of *β-catenin* RNA (Supp. Fig. 3B). Whereas this was not associated with significant elevation of the total number of transients, we note that high variability of the Ca^{2+} transients' frequency between individual embryos might have prevented detection of such an increase (Fig. 3A; Supp. Fig. 3B). In addition, we demonstrated that this dorsal-biased Ca^{2+} signaling lasts from 3 to 5 hpf, about twice as long as initially reported (Ma et al., 2009). Although the role of such dorsal-biased Ca^{2+} signaling after MBT is still unclear, it is possible that it functions in the establishment and/or maintenance of the dorsal organizer and the process of axis formation. Indeed, the diminished Ca^{2+} signaling bias in ventralized *ichabod/β-catenin2* mutant embryos and the increased frequency of Ca^{2+} signaling in induced dorsal organizer further support this notion (Fig. 4A-C). Together, our work strengthens an intriguing interaction between Ca^{2+} signaling and the Wnt/β-catenin pathway before and after MBT (Ma et al., 2009; Slusarski et al., 1997b; Wu et al., 2012), and offers a highly sensitive calcium reporter for future investigations of the underlying molecular mechanisms.

Recent studies have implicated DFC Ca^{2+} signaling in the regulation of zebrafish left-right patterning during gastrulation. Ca^{2+} sensor Fura-2 was employed to visualize localized Ca^{2+} signaling from the DFCs at 60–90% epiboly stages in lateral view of the gastrulae. Manipulation of Ca^{2+} release in the DFCs by thapsigargin treatment at the early to mid-gastrulation stages disrupts KV formation and randomizes organ laterality (Kreiling et al., 2008; Schneider et al., 2008). Analyzing *Tg[βactin2:GCaMP6s]*$^{stl351/stl351}$ gastrulae in dorsal view, we detected Ca^{2+} directly in the smaller, mesenchymal-like DFC cells in addition to the larger, epithelial-like EVL cells (Fig. 5A). Moreover, we found that Ca^{2+} transients in the DFCs display similar duration as those in EVL cells. Given that DFCs form by the ingression of dorsal margin EVL cells at the onset of epiboly (Oteiza et al., 2008), we speculate that the Ca^{2+} signaling activity in the DFCs might be a remnant of their EVL origins. As most of Ca^{2+} inhibition experiments were performed via treatments of whole embryos, it remains unclear whether Ca^{2+} transients in the DFCs have a specific role in the KV formation. Interestingly, we observed prolonged duration of Ca^{2+} transients specifically in the DFCs but not in the surrounding EVL cells in embryos in which Nodal signaling was elevated by injection of synthetic *cyc/ndr2* RNA at the cleavage stages, suggesting that Ca^{2+} signaling in DFCs and EVL cells can be differentially regulated. Whereas Ca^{2+} signaling modulation has been implicated in the regulation of Nodal gene expression during left-right patterning (Takao et al., 2013), whether Nodal signaling plays a role in controlling Ca^{2+} signaling directly or indirectly is unknown. Our data suggest that Nodal signaling is capable of modulating Ca^{2+} signaling specifically in the DFCs during gastrulation (Fig. 5B,C). Given that Nodal signaling promotes DFC formation in a cell non-autonomous manner (Oteiza et al., 2008), it is possible that Nodal signaling influences DFC Ca^{2+} transient duration also functioning cell non-autonomously. In support of this notion is our data that DFC Ca^{2+} transient duration remained unchanged when synthetic *cyc/ndr2* RNA was injected into the YSL after its separation from the blastoderm (Fig. 5B), what should directly activate Nodal signaling in DFCs (Amack and Yost, 2004; Cooper and D'Amico, 1996).

In conclusion, we leveraged GCaMP6s GECI to generate a superior Ca^{2+} indicator transgenic line, *Tg[βactin2:GCaMP6s]*$^{stl351/stl351}$, for improved *in vivo* Ca^{2+} imaging during early embryogenesis in zebrafish. We extended previous Ca^{2+} imaging studies with better spatial and temporal Ca^{2+} dynamics at the blastula and gastrulation stages. These transgenic Ca^{2+} indicator lines will enable investigating the mechanisms that restrict Ca^{2+} transients to the EVL cells and the specific roles and mechanisms of both the homogenous and dorsal-biased Ca^{2+} EVL cell signaling before and after the onset of zygotic transcription in the process of axis formation.

4. Materials and methods

4.1. Zebrafish lines and maintenance

Zebrafish embryos were collected from natural matings and maintained in egg water at 28.5 °C. Embryos were staged according to morphology (Kimmel et al., 1995). Wild-type (WT) strain AB* was used to generate the transgenic lines. All experiments and procedures were approved by the Animal Studies Committee of the Washington University School of Medicine.

4.2. Confocal imaging

Transgenic embryos were manually dechorionated at the described stages and mounted in 0.3% low melting agarose (Lonza) on a coverglass bottom dish. Z-stack time-lapse imaging was performed at 28.5 °C using a spinning-disk confocal microscope (Quorum) with a 491-nm wavelength laser. Time-lapse imaging was set up with 3 μm interval z stacks for a total of 50 slices and 15 s interval for EVL Ca^{2+} imaging, and 2 μm interval z stacks for a total of 20–30 slices and 10–15 s interval for DFC Ca^{2+} imaging. Gap junction inhibitor CBX was either applied at 50–100 μM final concentration directly to dechorionated embryos for 30 min before imaging or applied to the agarose-mounted embryos at 100 μM final concentration during imaging (Satou et al., 2009; Wang et al., 2014).

4.3. *Plasmids and* in vitro *Transcription*

The following constructs were used in this study: *pGF-CMV-GCaMP6s* (Chen et al., 2013), *pBH-R4/R2* (Heim et al., 2014), *p5E-bactin2*, *pCS2FA-transposase* (Kwan et al., 2007), *p5E-ubi* (Mosimann et al., 2011), *pCS2+wnt5b* (Lin et al., 2010), and *pCS2+cyc/ndr2* (Rebagliati et al., 1998). The *GCaMP6s* open reading frame (ORF) was amplified from *pGF-CMV-GCaMP6s* using Phusion High-Fidelity DNA polymerase (Invitrogen) with *GCaMP6s*-Forward and -Reverse primers (Table S1). The amplified *GCaMP6s* ORF was cloned into *pENTR/D-TOPO* (Invitrogen) and sequenced. To generate *Tol2* destination constructs, *p5E-βactin2* or *p5E-ubi* promoter sequences were recombined with *pENTR/D-GCaMP6s* into *pBH-R4/R2* using the Gateway LR Clonase II Plus enzyme (Invitrogen).

To generate *cyc/ndr2* RNA, *pCS2+cyc/ndr2* plasmid was linearized with *Asp718I*, purified (Qiagen), and used as a template for RNA synthesis with the mMessage mMachine SP6 kit (Ambion). The resulting RNA was purified with the Micro Bio-Spin P-30 columns (Bio-Rad). 50 pg *cyc/ndr-2* RNA mixed with 0.1% Texas Red was injected at 64-cell stage to 1–2 marginal blastomeres, or 400 pg was injected at 512-cell stage to the yolk cell. *pCS2+wnt5b* was linearized with *Apa*I, and transcribed and purified as described above. 50–100 pg *wnt5b* synthetic RNA was injected at 1-cell stage.

4.4. Quantitative PCR

To quantify the relative insertion copy number of *GCaMP6s DNA*, genomic DNA was extracted from the adult transgenic fish fin using the DNeasy Blood & Tissue Kit (Qiagen). To quantify the relative

GCaMP6s transcript levels, RNA was isolated from whole embryos using Trizol (Invitrogen) and subjected to cDNA preparation (SuperScript III, Invitrogen). Quantitative PCR (qPCR) was performed in CFX Connect Real time system (Bio-Rad) using the primers listed in Supplementary material Table S1.

4.4.1. Quantification of Ca^{2+} transients

Time-lapse movies (interval=15 s) were collected from 2.5 to 8 hpf, but a different embryo was replaced every 1.5–2.5 h to prevent phototoxicity or photobleaching. The embryonic shield was identified at around 6.5 hpf to retrospectively define the four quadrants (dorsal, ventral, left, and right) at blastula stages for the quantification of Ca^{2+} transients in each quadrant (Fig. 3B). Ca^{2+} transients were defined as previously described (Reinhard et al., 1995). The Fiji cell counter plugin (Schindelin et al., 2012) was used to manually quantify Ca^{2+} transients. Data were analyzed in Prism 6 software (GraphPad) using two-way ANOVA test.

For automated Ca^{2+} transient quantification, the raw movie was converted into ΔF/F0 version by calculating on each pixel:

$$\Delta F/F0 = \frac{F - F0}{F0}$$

where F is the current value of pixel, F0 is the mean of pixel values along the recording time. The contrast was enhanced between background and active cell. Each frame was divided into dorsal, ventral, right and left quadrants similar as manual quantification described above. Empirically, we chose 0.4–0.5 as a threshold level for each recording video to convert the video into binary frames. After that, all four-connected components fewer then 20 pixels were removed. Components remaining after removing were considered to be active cells. In order to capture individual cells, centroids of components were calculated and assigned into each sub-region. Centroids that had a distance less then 20 were considered the same cell. Additionally, a cell active in continuous two frames was counted only once. A Gaussian weight matrix was assigned to correct the size difference associated with the cell distribution:

$$weight(i, j) = (i - 0.5*a)^2 + (j - 0.5*b)^2$$

Where (i, j) is the centroid's coordinate. An estimated size for cells was calculated by

$$S(i, j) = S*weight(i, j)$$

Where S(i,j) is the estimated cell size on coordinates (i,j) and S is the center cell's size. Then each component was counted as:

$$N = Round\left(\frac{n}{S(i, j)}\right)$$

Where n is the number of pixels of the components. The number of cell activity events was counted separately for each sub-region. All the data for Wnt5b-overexpression, ventralized, and dorsalized embryos were quantified using the automated method. The resulting data were subjected to statistical analysis using Prism 6 software (GraphPad).

Author contributions

JC and LSK designed the experiments. JC performed the experiments and analyzed the data. LX and MRB developed the automated algorithm. All authors were involved in data interpretation and writing the manuscript.

Acknowledgements

We thank Gina Castelvecchi, Diane Sepich, Jimann Shin, Margot Williams and other members of the Solnica-Krezel lab for discussion and comments on the manuscript; and the Washington University School of Medicine in St. Louis Zebrafish Facility Staff for excellent animal care. We also thank Florence Marlow for *pBH-R4/R2*, Douglas Kim for *pGF-CMV-GCaMP6s*, and Diane Slusarski for *pCS2+wnt5b*. This work was supported in part by R01GM77770 and R35GM118179 grants to LSK, and EUREKA grant R01DA037152 to MRB from the National Institutes of Health.

Appendix A. Supporting information

Supplementary data associated with this article can be found in the online version at doi:10.1016/j.ydbio.2017.03.010.

References

Aanes, H., Winata, C.L., Lin, C.H., Chen, J.P., Srinivasan, K.G., Lee, S.G., Lim, A.Y., Hajan, H.S., Collas, P., Bourque, G., et al., 2011. Zebrafish mRNA sequencing deciphers novelties in transcriptome dynamics during maternal to zygotic transition. Genome Res. 21, 1328–1338.
Amack, J.D., Yost, H.J., 2004. The T box transcription factor no tail in ciliated cells controls zebrafish left-right asymmetry. Curr. Biol.: CB 14, 685–690.
Berridge, M.J., 1993. Inositol trisphosphate and calcium signalling. Nature 361, 315–325.
Berridge, M.J., Bootman, M.D., Roderick, H.L., 2003. Calcium signalling: dynamics, homeostasis and remodelling. Nat. Rev. Mol. Cell Biol. 4, 517–529.
Blaser, H., Reichman-Fried, M., Castanon, I., Dumstrei, K., Marlow, F.L., Kawakami, K., Solnica-Krezel, L., Heisenberg, C.P., Raz, E., 2006. Migration of zebrafish primordial germ cells: a role for myosin contraction and cytoplasmic flow. Dev. Cell 11, 613–627.
Campinho, P., Behrndt, M., Ranft, J., Risler, T., Minc, N., Heisenberg, C.P., 2013. Tension-oriented cell divisions limit anisotropic tissue tension in epithelial spreading during zebrafish epiboly. Nat. Cell Biol. 15, 1405–1414.
Chang, D.C., Meng, C., 1995. A localized elevation of cytosolic free calcium is associated with cytokinesis in the zebrafish embryo. J. Cell Biol. 131, 1539–1545.
Chen, T.-W.W., Wardill, T.J., Sun, Y., Pulver, S.R., Renninger, S.L., Baohan, A., Schreiter, E.R., Kerr, R.A., Orger, M.B., Jayaraman, V., et al., 2013. Ultrasensitive fluorescent proteins for imaging neuronal activity. Nature 499, 295–300.
Chi, N.C., Bussen, M., Brand-Arzamendi, K., Ding, C., Olgin, J.E., Shaw, R.M., Martin, G.R., Stainier, D.Y., 2010. Cardiac conduction is required to preserve cardiac chamber morphology. Proc. Natl. Acad. Sci. USA 107, 14662–14667.
Choi, W.Y., Giraldez, A.J., Schier, A.F., 2007. Target protectors reveal dampening and balancing of Nodal agonist and antagonist by miR-430. Science 318, 271–274.
Clapham, D.E., 1995. Calcium signaling. Cell 80, 259–268.
Clapham, D.E., 2007. Calcium signaling. Cell 131, 1047–1058.
Cooper, M.S., D'Amico, L.A., 1996. A cluster of noninvoluting endocytic cells at the margin of the zebrafish blastoderm marks the site of embryonic shield formation. Dev. Biol. 180, 184–198.
De Koninck, P., Schulman, H., 1998. Sensitivity of CaM kinase II to the frequency of Ca2+ oscillations. Science 279, 227–230.
Dolmetsch, R.E., Xu, K., Lewis, R.S., 1998. Calcium oscillations increase the efficiency and specificity of gene expression. Nature 392, 933–936.
Dreosti, E., Odermatt, B., Dorostkar, M.M., Lagnado, L., 2009. A genetically encoded reporter of synaptic activity in vivo. Nat. Methods 6, 883–889.
Dumollard, R., Sardet, C., 2001. Three different calcium wave pacemakers in ascidian eggs. J. Cell Sci. 114, 2471–2481.
Essner, J.J., Amack, J.D., Nyholm, M.K., Harris, E.B., Yost, H.J., 2005. Kupffer's vesicle is a ciliated organ of asymmetry in the zebrafish embryo that initiates left-right development of the brain, heart and gut. Development 132, 1247–1260.
Fluck, R.A., Miller, A.L., Jaffe, L.F., 1991. Slow calcium waves accompany cytokinesis in medaka fish eggs. J. Cell Biol. 115, 1259–1265.
Gallo, E.M., Cante-Barrett, K., Crabtree, G.R., 2006. Lymphocyte calcium signaling from membrane to nucleus. Nat. Immunol. 7, 25–32.
Garic-Stankovic, A., Hernandez, M., Flentke, G.R., Zile, M.H., Smith, S.M., 2008. A ryanodine receptor-dependent Ca(i)(2+) asymmetry at Hensen's node mediates avian lateral identity. Development 135, 3271–3280.
Gilkey, J.C., Jaffe, L.F., Ridgway, E.B., Reynolds, G.T., 1978. A free calcium wave traverses the activating egg of the medaka, Oryzias latipes. J. Cell Biol. 76, 448–466.
Gilland, E., Miller, A.L., Karplus, E., Baker, R., Webb, S.E., 1999. Imaging of multicellular large-scale rhythmic calcium waves during zebrafish gastrulation. Proc. Natl. Acad. Sci. USA 96, 157–161.
Groigno, L., Whitaker, M., 1998. An anaphase calcium signal controls chromosome disjunction in early sea urchin embryos. Cell 92, 193–204.
Harvey, S.A., Sealy, I., Kettleborough, R., Fenyes, F., White, R., Stemple, D., Smith, J.C., 2013. Identification of the zebrafish maternal and paternal transcriptomes. Development 140, 2703–2710.
Heim, A.E., Hartung, O., Rothhamel, S., Ferreira, E., Jenny, A., Marlow, F.L., 2014. Oocyte polarity requires a Bucky ball-dependent feedback amplification loop. Development 141, 842–854.
Jaenisch, R., Jahner, D., Nobis, P., Simon, I., Lohler, J., Harbers, K., Grotkopp, D., 1981. Chromosomal position and activation of retroviral genomes inserted into the germ line of mice. Cell 24, 519–529.
Kane, D.A., Kimmel, C.B., 1993. The zebrafish midblastula transition. Development 119, 447–456.
Kawakami, K., Shima, A., Kawakami, N., 2000. Identification of a functional transposase

of the Tol2 element, an Ac-like element from the Japanese medaka fish, and its transposition in the zebrafish germ lineage. Proc. Natl. Acad. Sci. USA 97, 11403–11408.
Kelly, C., Chin, A.J., Leatherman, J.L., Kozlowski, D.J., Weinberg, E.S., 2000. Maternally controlled (beta)-catenin-mediated signaling is required for organizer formation in the zebrafish. Development 127, 3899–3911.
Kelly, G.M., Erezyilmaz, D.F., Moon, R.T., 1995. Induction of a secondary embryonic axis in zebrafish occurs following the overexpression of beta-catenin. Mech. Dev. 53, 261–273.
Kimmel, C.B., Ballard, W.W., Kimmel, S.R., Ullmann, B., Schilling, T.F., 1995. Stages of embryonic development of the zebrafish. Dev. Dyn.: Off. Publ. Am. Assoc. Anat. 203, 253–310.
Kreiling, J.A., Balantac, Z.L., Crawford, A.R., Ren, Y., Toure, J., Zchut, S., Kochilas, L., Creton, R., 2008. Suppression of the endoplasmic reticulum calcium pump during zebrafish gastrulation affects left-right asymmetry of the heart and brain. Mech. Dev. 125, 396–410.
Kume, S., Muto, A., Inoue, T., Suga, K., Okano, H., Mikoshiba, K., 1997. Role of inositol 1,4,5-trisphosphate receptor in ventral signaling in Xenopus embryos. Science 278, 1940–1943.
Kwan, K.M., Fujimoto, E., Grabher, C., Mangum, B.D., Hardy, M.E., Campbell, D.S., Parant, J.M., Yost, H.J., Kanki, J.P., Chien, C.B., 2007. The Tol2kit: a multisite gateway-based construction kit for Tol2 transposon transgenesis constructs. Dev. Dyn.: Off. Publ. Am. Assoc. Anat. 236, 3088–3099.
Lee, K.W., Webb, S.E., Miller, A.L., 1999. A wave of free cytosolic calcium traverses zebrafish eggs on activation. Dev. Biol. 214, 168–180.
Lee, M.T., Bonneau, A.R., Takacs, C.M., Bazzini, A.A., DiVito, K.R., Fleming, E.S., Giraldez, A.J., 2013. Nanog, Pou5f1 and SoxB1 activate zygotic gene expression during the maternal-to-zygotic transition. Nature 503, 360–364.
Li, W., Llopis, J., Whitney, M., Zlokarnik, G., Tsien, R.Y., 1998. Cell-permeant caged InsP3 ester shows that Ca2+ spike frequency can optimize gene expression. Nature 392, 936–941.
Lin, S., Baye, L.M., Westfall, T.A., Slusarski, D.C., 2010. Wnt5b-Ryk pathway provides directional signals to regulate gastrulation movement. J. Cell Biol. 190, 263–278.
Lyman Gingerich, J., Westfall, T.A., Slusarski, D.C., Pelegri, F., 2005. hecate, a zebrafish maternal effect gene, affects dorsal organizer induction and intracellular calcium transient frequency. Dev. Biol. 286, 427–439.
Ma, L.H., Webb, S.E., Chan, C.M., Zhang, J., Miller, A.L., 2009. Establishment of a transitory dorsal-biased window of localized Ca2+ signaling in the superficial epithelium following the mid-blastula transition in zebrafish embryos. Dev. Biol. 327, 143–157.
Marsden, K.C., Granato, M., 2015. In vivo Ca(2+) imaging reveals that decreased dendritic excitability drives startle habituation. Cell Rep. 13, 1733–1740.
Maximiliano, L.S., Hiroshi, K., Akihiro, U., Kazuhide, A., Koichi, K., 2009. Transgenesis in zebrafish with the tol2 transposon system. Methods Mol. Biol., (Clifton, NJ).
McGrath, J., Somlo, S., Makova, S., Tian, X., Brueckner, M., 2003. Two populations of node monocilia initiate left-right asymmetry in the mouse. Cell 114, 61–73.
Miller, A.L., Fluck, R.A., McLaughlin, J.A., Jaffe, L.F., 1993. Calcium buffer injections inhibit cytokinesis in Xenopus eggs. J. Cell Sci. 106 (Pt 2), 523–534.
Miyawaki, A., Llopis, J., Heim, R., McCaffery, J.M., Adams, J.A., Ikura, M., Tsien, R.Y., 1997. Fluorescent indicators for Ca2+ based on green fluorescent proteins and calmodulin. Nature 388, 882–887.
Mosimann, C., Kaufman, C.K., Li, P., Pugach, E.K., Tamplin, O.J., Zon, L.I., 2011. Ubiquitous transgene expression and Cre-based recombination driven by the ubiquitin promoter in zebrafish. Development 138, 169–177.
Mosimann, C., Puller, A.C., Lawson, K.L., Tschopp, P., Amsterdam, A., Zon, L.I., 2013. Site-directed zebrafish transgenesis into single landing sites with the phiC31 integrase system. Dev. Dyn. 242, 949–963.
Mosimann, C., Zon, L.I., 2011. Advanced zebrafish transgenesis with Tol2 and application for Cre/lox recombination experiments. Methods Cell Biol. 104, 173–194.
Oancea, E., Meyer, T., 1998. Protein kinase C as a molecular machine for decoding calcium and diacylglycerol signals. Cell 95, 307–318.
Oteiza, P., Koppen, M., Concha, M.L., Heisenberg, C.P., 2008. Origin and shaping of the laterality organ in zebrafish. Development 135, 2807–2813.
Parry, H., McDougall, A., Whitaker, M., 2005. Microdomains bounded by endoplasmic reticulum segregate cell cycle calcium transients in syncytial Drosophila embryos. J. Cell Biol. 171, 47–59.
Randlett, O., Poggi, L., Zolessi, F.R., Harris, W.A., 2011. The oriented emergence of axons from retinal ganglion cells is directed by laminin contact in vivo. Neuron 70, 266–280.
Rebagliati, M.R., Toyama, R., Haffter, P., Dawid, I.B., 1998. cyclops encodes a nodal-related factor involved in midline signaling. Proc. Natl. Acad. Sci. USA 95, 9932–9937.
Reinhard, E., Yokoe, H., Niebling, K.R., Allbritton, N.L., Kuhn, M.A., Meyer, T., 1995. Localized calcium signals in early zebrafish development. Dev. Biol. 170, 50–61.
Roberts, J.A., Miguel-Escalada, I., Slovik, K.J., Walsh, K.T., Hadzhiev, Y., Sanges, R., Stupka, E., Marsh, E.K., Balciuniene, J., Balciunas, D., et al., 2014. Targeted transgene integration overcomes variability of position effects in zebrafish. Development 141, 715–724.
Romoser, V.A., Hinkle, P.M., Persechini, A., 1997. Detection in living cells of Ca2+-dependent changes in the fluorescence emission of an indicator composed of two green fluorescent protein variants linked by a calmodulin-binding sequence. A new class of fluorescent indicators. J. Biol. Chem. 272, 13270–13274.
Runft, L.L., Jaffe, L.A., Mehlmann, L.M., 2002. Egg activation at fertilization: where it all begins. Dev. Biol. 245, 237–254.
Sampath, K., Rubinstein, A.L., Cheng, A.M., Liang, J.O., Fekany, K., Solnica-Krezel, L., Korzh, V., Halpern, M.E., Wright, C.V., 1998. Induction of the zebrafish ventral brain and floorplate requires cyclops/nodal signalling. Nature 395, 185–189.
Sarmah, B., Latimer, A.J., Appel, B., Wente, S.R., 2005. Inositol polyphosphates regulate zebrafish left-right asymmetry. Dev. Cell 9, 133–145.
Satou, C., Kimura, Y., Kohashi, T., Horikawa, K., Takeda, H., Oda, Y., Higashijima, S., 2009. Functional role of a specialized class of spinal commissural inhibitory neurons during fast escapes in zebrafish. J. Neurosci. 29, 6780–6793.
Schindelin, J., Arganda-Carreras, I., Frise, E., Kaynig, V., Longair, M., Pietzsch, T., Preibisch, S., Rueden, C., Saalfeld, S., Schmid, B., et al., 2012. Fiji: an open-source platform for biological-image analysis. Nat. Methods 9, 676–682.
Schneider, I., Houston, D.W., Rebagliati, M.R., Slusarski, D.C., 2008. Calcium fluxes in dorsal forerunner cells antagonize beta-catenin and alter left-right patterning. Development 135, 75–84.
Schneider, S., Steinbeisser, H., Warga, R.M., Hausen, P., 1996. Beta-catenin translocation into nuclei demarcates the dorsalizing centers in frog and fish embryos. Mech. Dev. 57, 191–198.
Slusarski, D.C., Corces, V.G., Moon, R.T., 1997a. Interaction of Wnt and a Frizzled homologue triggers G-protein-linked phosphatidylinositol signalling. Nature 390, 410–413.
Slusarski, D.C., Yang-Snyder, J., Busa, W.B., Moon, R.T., 1997b. Modulation of embryonic intracellular Ca2+ signaling by Wnt-5A. Dev. Biol. 182, 114–120.
Solnica-Krezel, L., Stemple, D.L., Mountcastle-Shah, E., Rangini, Z., Neuhauss, S.C., Malicki, J., Schier, A.F., Stainier, D.Y., Zwartkruis, F., Abdelilah, S., et al., 1996. Mutations affecting cell fates and cellular rearrangements during gastrulation in zebrafish. Development 123, 67–80.
Steinhardt, R., Zucker, R., Schatten, G., 1977. Intracellular calcium release at fertilization in the sea urchin egg. Dev. Biol. 58, 185–196.
Streb, H., Irvine, R.F., Berridge, M.J., Schulz, I., 1983. Release of Ca2+ from a nonmitochondrial intracellular store in pancreatic acinar cells by inositol-1,4,5-trisphosphate. Nature 306, 67–69.
Takao, D., Nemoto, T., Abe, T., Kiyonari, H., Kajiura-Kobayashi, H., Shiratori, H., Nonaka, S., 2013. Asymmetric distribution of dynamic calcium signals in the node of mouse embryo during left-right axis formation. Dev. Biol. 376, 23–30.
Tallini, Y.N., Ohkura, M., Choi, B.R., Ji, G., Imoto, K., Doran, R., Lee, J., Plan, P., Wilson, J., Xin, H.B., et al., 2006. Imaging cellular signals in the heart in vivo: cardiac expression of the high-signal Ca2+ indicator GCaMP2. Proc. Natl. Acad. Sci. USA 103, 4753–4758.
Uchida, S., Yamada, S., Deguchi, Y., Yamamoto, M., Kimura, R., 2000. In vivo specific binding characteristics and pharmacokinetics of a 1,4-dihydropyridine calcium channel antagonist in the senescent mouse brain. Pharm. Res 17, 844–850.
Wallingford, J.B., Ewald, A.J., Harland, R.M., Fraser, S.E., 2001. Calcium signaling during convergent extension in Xenopus. Curr. Biol.: CB 11, 652–661.
Wang, T.M., Holzhausen, L.C., Kramer, R.H., 2014. Imaging an optogenetic pH sensor reveals that protons mediate lateral inhibition in the retina. Nat. Neurosci. 17, 262–268.
Webb, S.E., Lee, K.W., Karplus, E., Miller, A.L., 1997. Localized calcium transients accompany furrow positioning, propagation, and deepening during the early cleavage period of zebrafish embryos. Dev. Biol. 192, 78–92.
Webb, S.E., Miller, A.L., 2003. Calcium signalling during embryonic development. Nat. Rev. Mol. Cell Biol. 4, 539–551.
Westfall, T.A., Brimeyer, R., Twedt, J., Gladon, J., Olberding, A., Furutani-Seiki, M., Slusarski, D.C., 2003a. Wnt-5/pipetail functions in vertebrate axis formation as a negative regulator of Wnt/beta-catenin activity. J. Cell Biol. 162, 889–898.
Westfall, T.A., Hjertos, B., Slusarski, D.C., 2003b. Requirement for intracellular calcium modulation in zebrafish dorsal-ventral patterning. Dev. Biol. 259, 380–391.
Whitaker, M., 2006. Calcium at fertilization and in early development. Physiol. Rev. 86, 25–88.
Wilson, C., Bellen, H.J., Gehring, W.J., 1990. Position effects on eukaryotic gene expression. Annu. Rev. Cell Biol. 6, 679–714.
Wu, S.-Y.Y., Shin, J., Sepich, D.S., Solnica-Krezel, L., 2012. Chemokine GPCR signaling inhibits β-catenin during zebrafish axis formation. PLoS Biol. 10.
Yin, V.P., Lepilina, A., Smith, A., Poss, K.D., 2012. Regulation of zebrafish heart regeneration by miR-133. Dev. Biol. 365, 319–327.
Yuan, S., Zhao, L., Brueckner, M., Sun, Z., 2015. Intraciliary calcium oscillations initiate vertebrate left-right asymmetry. Curr. Biol.: CB 25, 556–567.